24th INTERNATIONAL CONGRESS ON SOUND AND VIBRATION
23–27 July 2017, London

OPTIMAL PLACEMENT OF SIX INERTIAL MASS ACTUATORS FOR MIMO ACTIVE VIBRATION CONTROL ON A LABORATORY TRUSS STRUCTURE

Giovanni Lapiccirella and Jens Rohlfing

Fraunhofer Institute for structural durability and system reliability LBF, Darmstadt, Germany
email: giovanni.lapiccirella@lbf.fraunhofer.de

Maryam Ghandchi Tehrani

University of Southampton, ISVR, Highfield, Southampton, UK

Large flexible structures require a system comprising multiple actuators and sensors in order to efficiently control multiple structural modes. Controllability and observability are important properties to take into account when designing such a multiple-input multiple-output (MIMO) active vibration control (AVC) system. The actuator placement may influence the control performance, stability and energy efficiency of the control system. The actuators need to efficiently excite the dominant structural modes in order to achieve the desired control performance and minimize the effort.

This work presents a practical analysis for the placement of six inertial mass actuators (IMAs) on a laboratory truss structure. A reduced order state space model of the truss structure is derived from a finite element (FE) model. Fourteen possible actuator mounting locations are considered. First, the problem of choosing the optimal placement for a single actuator is investigated and discussed. The problem is then extended to a system with six actuators. Possible optimal actuator placements are derived for the control of the dominant structural modes in a defined frequency range.

A decentralized MIMO velocity feedback control with six IMAs is applied to the truss structure in order to assess the control performance, stability and power consumption. For simplicity, it is assumed that all IMAs have identical electro-mechanical characteristics. The control stability is discussed based on the analysis of the systems open-loop frequency response functions (OL-FRFs) using the generalized Nyquist criterion. The active control performance and the electrical power consumption of the control system for selected actuator arrangements is evaluated and compared. It is found that an optimal actuator arrangement can be identified using a performance index (PI). Arrangements with high PI guarantee good control performance and relatively lower power consumption. The analysis presented is independent of the location of the primary disturbance force on the truss structure.

Keywords: Active vibration control, optimal placement, actuators, controllability

1. Introduction

Large flexible structures require distributed AVC systems for the control of multiple vibration modes. The placement of the actuators on the structure may influence the control performance, stability and power consumption of the system. The controllability of the dominant structural modes at specific locations on the structure is an important criterion when choosing where to place actuators. Since the concept of controllability has been introduced by Kàlman [1], several scalar measures have been proposed to assess the controllability of structures at predefined locations.

If a state space representation is used to describe the dynamics of the structure, the information needed to assess the controllability is contained in the A and B matrices. A convenient mathematical method to assess the system controllability is represented by controllability gramian matri-

ces [2]. These matrices can be evaluated from the A and B matrices of a state space model. Most of the scalar controllability measures that can be found in the literature are based on them.

In a state space formulation a primary disturbance force can be included in the B matrix. This allows calculating the disturbance controllability gramians. Those special forms lead to cost functions allowing the evaluation of optimal actuator placements for specific disturbances [3]. It is usually found that optimal locations are those closest to the primary disturbance. However, the position and characteristics of external disturbances are not known for many applications.

Many of the cost functions in literature are either defined to find the positions where the actuator forces are maximized [4] or the control effort (i.e. power consumption) is minimised [5], [6]. These two approaches lead to similar results, if spillover effects on the residual modes are excluded from the analysis. Bruant et al. [7] proposed modifications of classical cost functions, in order to include the residual modes. The modified cost functions find actuator positions that minimise the spillover effects on the residual modes. However, the modified cost functions require a more complete model of the analysed structure.

In the literature, solutions tailored to specific problems have been also proposed. Lim [8] proposes a method for finding the intersection of the controllable and observable subspaces. This method is particularly suitable to define optimal positions for decentralised feedback control applications. Hamdan et al. [9] use the angles between the A matrix left eigenvectors and the B matrix as controllability measure for first and second order systems. Each angle defines the degree of controllability for single modes at each location. However, the method is computationally expensive when large number of modes and locations are investigated.

This paper presents simulation studies on the optimal placement of six IMAs for a decentralised velocity feedback AVC system on laboratory truss structure. A controllability criterion [5] is applied to a state space formulation of the reduced order model of the truss structure. The AVC system control stability, performance and power consumption is evaluated and compared for the different IMA arrangements.

2. Truss structure and the reduced model

Fig. 1a shows the investigated laboratory truss structure with the six electrodynamic IMAs. The truss structure is composed of 28 nodes, connecting 52 short and 24 long struts. The structure is mounted on low stiffness rubber mounts at the four principal corners. This guarantees that all the rigid body modes of the structure lie below 16 Hz. The first six global modes occur within the frequency range from 50 Hz to 161.5 Hz. A more detailed description of the structure and results of an experimental modal analysis are given in Ref. [10] and [11].

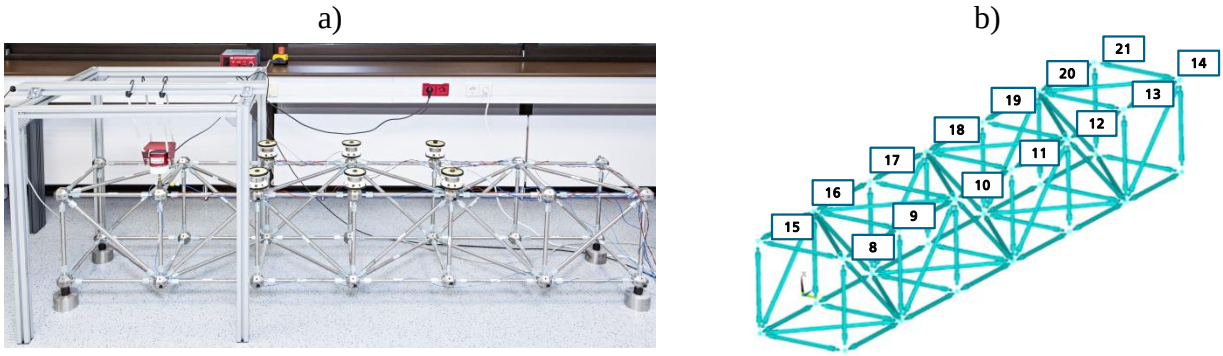

Figure 1: a) Laboratory six cells truss structure b) FEM model of the six cells truss structure

Fig. 1b shows the FE mode of the truss structure. This model has been validated in Ref. [11]. The model consists of more than 33000 degrees of freedom (DOF). The stiffness and the damping values of the connection points are set in order to the fit the experimentally evaluated torque values.

For the numerical analysis, FE model reduced to a model with a lower number of DOFs and then converted to a state-space formulation in the form described in Ref. [12].

3. Optimal placement of inertial mass actuators

3.1 Performance index

In this study, the method proposed by Hàc et al. [5] has been used to define the performance index (PI). In the case that a persistent disturbance acts on the system, the PI for *N* structural modes is defined as:

$$PI = 2(\sum_{i=1}^{N} E_i)\sqrt[N]{\prod_{i=1}^{N}(E_i)}, \quad (1)$$

where E_i is the total energy contribution (kinetic and potential) of the structure due to each ith vibrational mode. This energy contribution is given by

$$E_i = \beta_{ii}/4\zeta_i\omega_i\,; \quad \beta_{ii} = \sum_{q=1}^{k}\phi_i^2(P_q), \quad (2)$$

where ζ_i is the modal damping, ω_i is the eigenfrequency and $\phi_i^2(P_q)$ refers to the ith eigenvector squared value at the P_q spatial coordinate where an actuator is installed. The PI from Eq. (1) provides equal importance to all modes included in the analysis. The first term on the right hand side of Eq. (1) can be interpreted as the total energy of the system excited by the actuators. The term under the root sign tends to vanish if the controllability of any mode is lost. This ensures that none of the modes is nearly uncontrollable.

3.2 Optimal positions and optimal actuator arrangements

For the purpose of this study, the model of the truss structure has been reduced to 60 modes, which occur in the frequency range between 0 and 250 Hz. The input and output points are selected to be the fourteen connecting nodes on the top of the truss structure, numbered as shown in Fig. 1b. The reduced model is imported into Matlab as state space model using the mechanical simulation toolbox developed at the Fraunhofer LBF [13]. The PI is evaluated individually for each of the selected input/output points. The highest PIs are evaluated for positions 8, 14, 15 and 21 at the four principle corner positions of the truss structure. The lowest PIs are evaluated for positions 11 and 18 in the middle of the truss structure. The results are summarized in Table 1.

Table 1: Performance index of the single node positions

	Node positions														
	8	**9**	**10**	**11**	**12**	**13**	**14**	**15**	**16**	**17**	**18**	**19**	**20**	**21**	
PI	12	5,5	3,8	0	3,8	5,5	12	11	5,6	3,7	0	3,7	5,6	11	$\cdot 10^{-8}$

A second analysis considers a total of six actuators applied on the truss structure. The arrangement of six actuators in fourteen possible positions results in 3003 possible variations. The results for the selected actuator arrangements are given in Table 2. The Xs indicate the positions occupied by actuators. The first four rows show the actuator arrangements with the highest overall PIs. The last three rows show the actuator arrangements with the lowest overall PIs. All arrangements with high PI include actuators at nodes 8, 14, 15 and 21, which have a high individual PI (see Table 1). The two arrangements with the lowest PI include the node positions 11 and 18, which are the points with the lowest individual PI (see Table 1). These results indicate that an optimal actuator arrangement may be found by combining locations with high individual PI. However, the actuator arrangements with the highest PI also include positions 10 and 12. Those locations have lower individual than positions 9 and 13, which are not included in the top four results.

Table 2: Actuator placements with the highest PI (first four) and the lowest PI (last two).

	Node positions														PI
N°	**8**	**9**	**10**	**11**	**12**	**13**	**14**	**15**	**16**	**17**	**18**	**19**	**20**	**21**	
760	X		X				X	X	X					X	$6.62\ 10^{-6}$
770	X		X				X	X					X	X	$6.62\ 10^{-6}$
1096	X				X		X	X	X					X	$6.62\ 10^{-6}$
1106	X				X		X	X					X	X	$6.62\ 10^{-6}$
2099			X	X	X	X				X		X			$2.25\ 10^{-6}$
2154			X	X	X					X	X	X			$1.64\ 10^{-6}$

4. Active vibration control with optimal placement

In this section the control stability, performance and power consumption is evaluated for a MIMO decentralised velocity feedback AVC system with six voltage driven electrodynamic IMAs. A discussion of the electro – mechanical characteristics of the IMAs can be found in Ref. [14].

4.1 Stability analysis

The AVC system is only conditionally stable due to the interaction between the dynamic characteristics of the IMAs and the rigid body modes of the truss structure. The IMA's blocked force FRFs show a 180° phase drop around their resonance frequency. Moreover, if the IMAs are driven by a voltage, the phase of the blocked force FRF converges to -90° with increasing frequency. This leads to undesired spillover effects, which compromise the stability and performance of the control system. A phase lead/lag compensator has been designed in order to improve the control stability and system performance [14].

First the stability of the feedback loops at each location is studied individually using the Nyquist criterion. According to the Nyquist criterion, the system is stable if the OL-FRF does not encircle the Nyquist point [-1 0j]. The stable gain margins are assessed for each possible IMA position. These values are the highest gains that can be implemented. Usually, half of the maximum stable gains that guarantee a 6 dB gain margin are considered in the literature. However, a feedback gain that guarantees a 6 dB gain margin can lead to excessive control spillover. A more conservative measure is the 6 dB spillover gain, which is introduced here. The 6 dB spillover gain limits the system to a maximum spillover of 6 dB. This criterion is met when the OL-FRF is tangent to the circle with radius 0.5 around the Nyquist point as shown in Fig. 2. The stable gain margin and the 6 dB spillover gains at each location are given in Table 3. The results indicate that the 6 dB spillover gain is about a magnitude lower than the stable gain margin. It is interesting to note that positions 8, 14, 15 and 21 have the lowest stable gain margins. Those positions coincide with the highest PI locations in Table 1. Positions 11 and 18 show highest stable gain margins and lowest PIs.

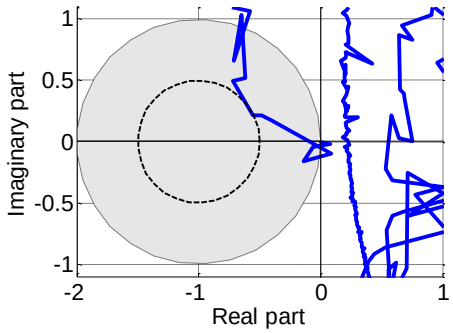

Figure 2: Nyquist plot of the OL-FRF at node 10 with 6 dB control spillover gain.

Table 3: Gain margin and 6 dB spillover gains at each single node position

	Nodes														
	8	**9**	**10**	**11**	**12**	**13**	**14**	**15**	**16**	**17**	**18**	**19**	**20**	**21**	
$\mathbf{G_{6dB}}$	2.1	5.2	5.9	5.4	5.9	5,2	2,1	2,2	5,1	5,9	5,1	5,9	5,1	2,2	$\cdot 10^4$
$\mathbf{G_{stable}}$	4.4	5.4	6.3	6.6	6.3	5.4	4.4	4.4	5.4	6.3	6.6	6.3	5.4	4.4	$\cdot 10^5$

The classical Nyquist criterion is not sufficient to assess the control stability of a decentralised MIMO system. The robustness of the system usually decreases with the number of actuators used. This is due to the cross excitation effects between the individual feedback loops [15]. Therefore, the stability of the decentralised MIMO system needs to be assessed using the generalised Nyquist criterion [16]. According to this criterion, none of the frequency dependent eigenvalues of the fully populated OL-FRFs $\boldsymbol{H}$ matrix must not encircle the Nyquist point [-1 0j]. The $\boldsymbol{H}$ matrix is evaluated by taking the OL-FRFs between the IMA input signals and the velocity output signals at all node positions where feedback loops are located. The stability of the MIMO system is limited by the eigenvalues with the lowest gain margin.

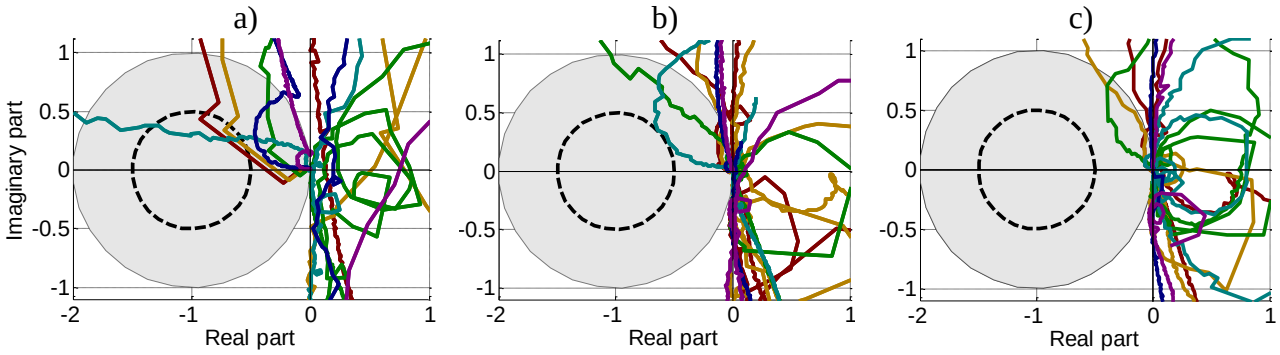

Figure 3: Nyquist plots of the OL-FRF matrix eigenvalues for the actuator arrangement 760, a) individual 6 dB spillover gains b) 6 dB spillover in the generalised Nyquist c) uniform minimal stable gain.

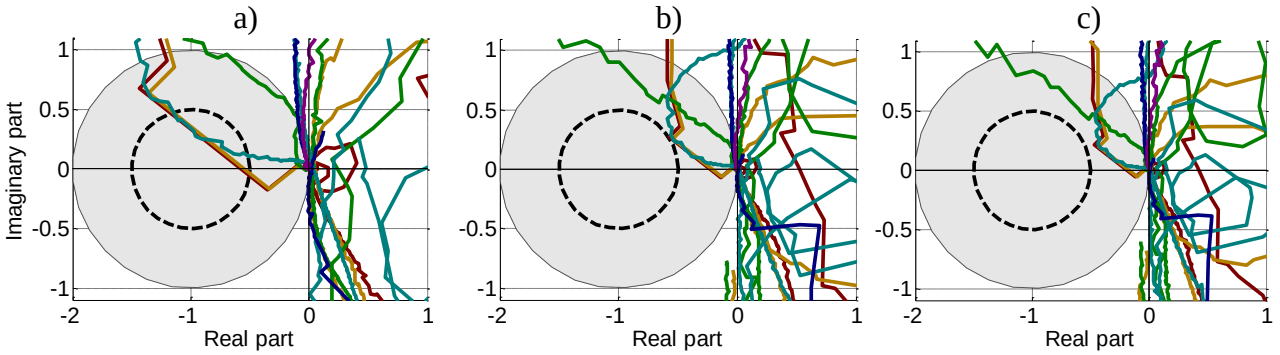

Figure 4: Nyquist plots of the OL-FRF matrix eigenvalues for the actuator arrangement 2154, a) individual 6 dB spillover gains b) 6 dB spillover in the generalised Nyquist c) uniform minimal stable gain.

In this study, different gain settings have been analysed for the different IMA arrangements presented in Table 2. For brevity, only the result for arrangements 760 and 2154 are presented here. Different cases of feedback gain settings have been considered. For brevity only three gain settings are discussed here. For case a) the gains of all feedback loops are set to the individual 6 dB spillover gains identified for the different locations. For case b) these gains are scaled uniformly in order to achieve the 6 dB spillover criterion in the generalised Nyquist. For case c), first the gains from case a) are uniformly scaled in order to achieve the 6 dB stability criterion in the generalised Nyquist; then the lowest of all individual gains is identified, finally all gains are set to this value.

Figs. 3 and 4 show the generalised Nyquist plots for the IMA arrangements 760 and 2154 for cases a), b) and c), respectively. The results in Fig. 3a and 4a show that the gain setting that gives 6

dB control spillover for the individual feedback loops results in a stable MIMO control system. However, the 6 dB spillover criterion is not satisfied in the generalised Nyquist. For the arrangement 760 with high PI in Fig. 3a, this gain setting results in a stable gain margin of more than 6 dB. This practically means that the eigenvalues of the OL-FRF matrix are crossing the negative real axis of the Nyquist plot outside the circle with radius 0.5 around the Nyquist point. For the arrangement 2154 with low PI in Fig. 4a, this gain setting also results in a stable control system. However, the gain margin is significantly less than 6 dB, i.e. the eigenvalues of the OL-FRF matrix are crossing the negative real axis of the Nyquist plot inside the circle with radius 0.5 around the Nyquist point.

For case b), the gains for the arrangement 760 in Fig. 3b have been uniformly scaled by a factor of 13% in order to satisfy the 6 dB spillover criterion in the generalised Nyquist. For the results of arrangement 2154 in Fig. 4b, all gains have been uniformly scaled by a factor of 40% to satisfy the 6dB spillover criterion. Figs. 3c and 4c show the results for case c). For both arrangements, all the feedback gains are set to a value of $2.21 \cdot 10^5$. However, the IMA arrangement 760 of Fig. 3c shows higher stability than actuator arrangement 2154 of Fig. 4c.

From case a) to case c) the gain setting is increasingly conservative. Hence, the control system set to the uniform gain in case c) results in a control system with the highest stability. However, control stability may come with a significant loss on the control performance. Hence, the closed loop control performance for the three cases is analysed in the section below. In order to compare the control performance for the two arrangements and three cases, the resulting power consumption and the resulting stroke of the IMA's proof mass is also evaluated.

4.2 Performance and power consumption

The control performance for the two IMA arrangements and the cases studied are evaluated in terms of the mean kinetic energy reductions in the frequency range between 0 Hz and 250 Hz. Reduction is evaluated as

$$R = \frac{\overline{E_k}}{\overline{E_{k_0}}} \qquad \text{and} \qquad \overline{E_{k,k0}} = \sum_{i=8}^{21} m_i v_i^2 \,/2T, \tag{3}$$

where $\overline{E_{k0}}$ refers to the total mean kinetic energy of the uncontrolled truss structure calculated using the velocities v_i of the fourteen nodes in x- direction, and where $\overline{E_k}$ is the total mean kinetic energy of the truss structure with applied active control. The power consumption of the AVC system is assessed summing the apparent power provided to the IMAs. In this analysis, the power amplifiers are assumed to be ideal voltage sources. The percentages of reactive power are also estimated. The reactive power component corresponds to the power oscillating between the power amplifier and actuators, without producing any active work. Results with high percentages of reactive power indicate that the power consumption may be reduced by using suitable power amplifiers, able to recuperate reactive power. Finally, the maximum stroke of the actuators is evaluated. If the linear stroke limit of the actuators of 5 mm is exceeded, the system cannot be implemented for the excitation level applied. For this study, the system is excited with a low pass filtered white noise signal with an RMS value of 6.87 N applied at node 9 (see Fig. 1b).

Fig. 5 shows the velocity spectra averaged over all 14 nodes normalized to the excitation force spectrum for the two IMA arrangements 760 and 2154 and for the three gain setting cases considered. Figs. 5a), 5b) and 5c) show the results for the cases a), b) and c), respectively. The normalized mean velocity is assumed to be proportional to the total kinetic energy of the truss structure.

In case a), the gain setting produces 6 dB spillover around 0.75 Hz for both IMA arrangements considered. However, higher reductions are achieved by the IMA arrangement 760.

The gain setting of case b) does not produce significant control spillover effects for any of the IMA arrangements considered. Higher reductions are achieved with the arrangement 2154, which is the arrangement with low PI.

Finally, the gain setting of case c) produces approximately 3 dB spillover at 0.75 Hz for both actuator arrangements. However, higher overall reductions are achieved with the IMA arrangement 760. The single value results are given in Table 4.

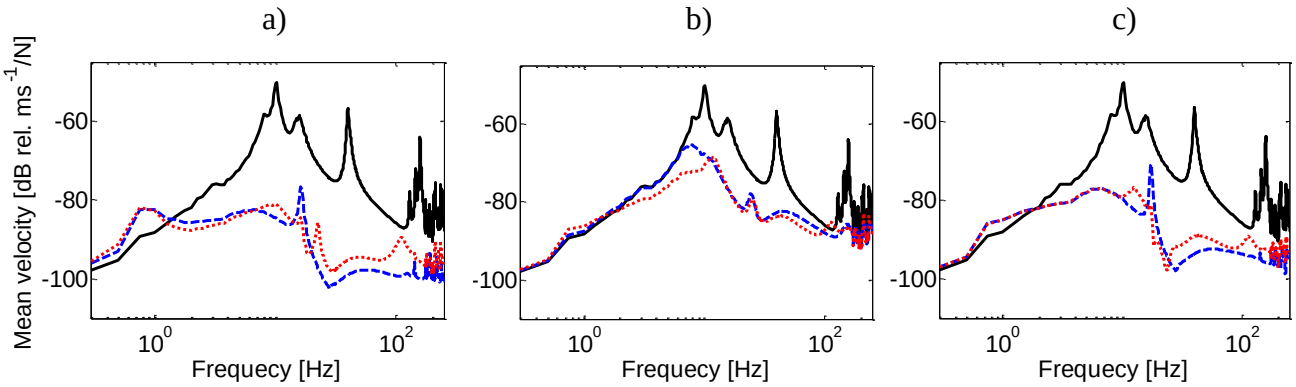

Figure 5: Mean velocity normalised to the excitation force. Uncontrolled structure (black continuous lines), IMA placement 760 (blue dashed line), IMA placement 2154 (red dotted lines); a) individual 6 dB spillover gains b) 6 dB spillover in the generalised Nyquist c) uniform minimal stable gain

Table 4 also summarises the results for the apparent power consumption, reactive power percentages and the maximum IMA stroke for all the six IMA placements considered in Table 2 and the three gain setting cases considered. The results for case a) show that the IMA arrangements with high PI achieve higher reductions with lower power consumptions and higher percentages of reactive power. For the primary excitation level considered, the maximum IMA stroke is close to the linear limit for all IMA arrangements considered. The results for case b) show higher reductions for IMA arrangements with low PI. The difference in the reductions between the best low PI arrangement (2099) and the best high PI arrangement (760) is about 1.5 dB. However, for the IMA arrangements with low PI the power consumption is two orders of magnitude higher in this case. The percentages of reactive power are approximately the same as those for case a). The maximum IMA stroke is within the linear limits for all IMA arrangements considered. The highest IMA stroke is evaluated for the IMA arrangements 2099 and 2154. The results for case c) show that the power consumption is in the same order of magnitude for all the IMA arrangements considered. However, the achieved control reductions for IMA arrangements with high PI are considerably higher than for those with low PI. The percentages of reactive power are slightly higher for high PI arrangements compared to cases a) and b). The IMA arrangements with low PI show approximately the same percentages of reactive power as in the gain setting cases a) and b). The maximum IMA strokes for all the IMA arrangements are within the linear limits.

Table 4: Simulation results for cases a), b) and c) for the six IMA arrangements from Table 2.

		Reductions [dB]			Apparent power [VA]			Reactive power [%]			Maximum Stroke [mm]		
		Cases			Cases			Cases			Cases		
		a)	b)	c)	a)	b)	c)	a)	b)	c)	a)	b)	c)
Arrangements	760	18.3	10.6	16.6	39.4	0.55	7.6	16.1	16.1	21.1	5	0.7	2
	770	18.3	10.2	16.6	39.5	0.5	7.6	16.2	16.2	21.1	5	0.6	2
	1096	17	9.4	15.7	26	0.4	6.5	10.1	10.1	19.6	4	0.5	2
	1106	17.1	8.8	15.8	26	0.4	6.5	10.2	10.2	19.6	4	0.5	2
	2099	14.5	12.1	11.2	107	11.6	7.2	6.1	6.71	6.7	4.2	2	1.6
	2154	12.7	10.7	10	81.6	9.5	5.9	7.6	8.1	8.13	3.7	2.1	1.6

5. Conclusions and Outlook

The results presented in this paper indicate that AVC systems with optimal actuator placements can achieve better control performance with lower power consumption. Actuator placements with

higher PI are also more stable. Moreover, high PI arrangements show a higher percentage of apparent power that may be recuperated using suitable power amplifiers. The IMA maximum strokes mainly depend on the primary excitation level and the feedback gain setting.

These results are part of an ongoing work. In future studies, it is intended to investigate AVC systems composed of six inertial mass actuators applying different control strategies (e.g. Velocity Feedback, Feedforward or Internal model control) on the laboratory truss structure introduced in this paper. The possibilities of centralised or decentralised architectures will be investigated in terms of control performance and power consumption. At this stage, the results suggest the importance of considering a holistic model of the AVC system in order to evaluate the performance and power consumption of the system.

6. Acknowledgements

The authors gratefully acknowledge the European Commission for its support of the Marie Sklodowska-Curie program through the ITN ANTARES project (GA 606817).

References

1 R. E. Kalman, Y. C. Ho und K. S. Narenda, „Controllability of linear dynamical systems," in *Contribution to Differential Equations*, 1962, pp. 189 - 213.

2 W. K. Gawronski, „Controllability and Observability," in *Advanced structural dynamics and active control of structures*, Pasadena, CA, USA, Springer, 1998, pp. 65-108.

3 M. A. Mirza und J. L. Van Niekerk, „Optimal Actuator Placement for Active Vibration control with known Disturbances," *Journal of Vibration and Control*, pp. 709 - 724, 1999.

4 Q. Wang und C. M. Wang, „A Controllability index for Optimal design of Piezoelectric Actuators in Vibration Control of Beam Structures," *Journal of Sound and Vibration*, pp. 507-518, 2000.

5 A. Hac und L. Liu, „Sensor and Actuator Location in Motion Control of Flexible Structures," *Journal of sound and vibrations*, pp. 239-261, 1993.

6 S. Herold, D. Mayer, J. Thiel, C. Schäfer und G. L. Stein, „Optimization and realization of distributed vibration absorbers," 2014.

7 I. Bruant und L. Proslier, „Optimal Location of Actuators and Sensors in Active Vibration Control," *Journal of Intelligent Material Systems and Structures*, pp. 197 - 206, 2005.

8 K. B. Lim, „Method for Optimal Actuator and Sensor Placement for Large Felxible Strucutres," *Journal of guidance*, pp. 49 - 57, 1992.

9 A. M. A. Hamdan und A. H. Nayfeh, „Measures of modal controllability and observability for First and Second order Linear System," *Journal of Guidance*, pp. 421 - 428, 1989.

10 D. Flaschenträger, J. Thiel, J. Rausch, H. Atzrodt, S. Herold, T. Melz und R. Wethschützky, „Implementation and Characterisation of the Dynamic Behaviour of a Three - Dimensional Truss Structure for Evaluatiing Smart Devices," in *ISMA 2010*, Leuven, 2010.

11 D. Mayer, H. Stoffregen, O. Heuss, J. Pöllmann, E. Abele und T. Melz, „Additive Manufacturing of Active Struts for Piezoelectric Shunt Damping," *Journal of Intelligent Material Systems and Structures*, pp. 1 -12, 2015.

12 S. Herold, W. Kaal und T. Melz, „Novel Dielectric stack actuators for dynamic applications," in *ASME 2012*, Stone Mountain, 2012.

13 F. LBF, „Mechanical Simulation Toolbox," Fraunhofer LBF, 2017. [Online]. Available: http://www.mechanical-simulation.de/joomla/index.php/de. [Zugriff am 1 2017].

14 G. Lapiccirella, J. Rohlfing und D. Mayer, „Performance and constraints of an active vibration control system with electrodynamic inertial mass actuators," in *ISMA and USD 2016*, Leuven, 2016.

15 O. N. Baumann und S. J. Elliott, „The stability of decentralized multi channel velocity feedback controllers using inertial actuator," *Journal of the Acoustical Society of America*, Bd. 1, Nr. 121, pp. 188 - 196, 2007.

16 J. M. Maciejowski, Multivariable Feedback Design, Cambridge, 1989.